Theor Chem Acc (2011) 128:569–577
DOI 10.1007/s00214-010-0792-9

REGULAR ARTICLE

A variational transition state theory description of periselectivity effects on cycloadditions of ketenes with cyclopentadiene

Juan Manuel Ramírez-Anguita · Ricard Gelabert · Àngels González-Lafont · Miquel Moreno · José M. Lluch

Received: 8 July 2010 / Accepted: 2 August 2010 / Published online: 20 August 2010

Abstract The reaction of cycloaddition of ketene and cyclopentadiene presents experimentally a competing mechanism where the branching ratio between the Woodward–Hoffmann allowed [4+2] and forbidden [2+2] cycloaddition product is 4.56 at −20 °C, but because the minimum energy path misses the [2+2] product altogether, it has been claimed to lie beyond the scope of transition state theory. In this paper, a variational transition state theory study on this reaction is presented. It is found that the minimum energy path affording the [4+2] product travels through a potential energy plateau very close to the minimum energy path that describes the interconversion between both cycloaddition products, allowing the transfer between both and the direct formation of the forbidden [2+2] product, in this way acting as a means to circumvent the Woodward–Hooffmann rules. Within the domain of the competitive canonical unified statistical theory, a value for the branching ratio in very good agreement with experiment is computed.

Keywords Variational transition state theory · Woodward–Hoffmann rules · Non-symmetrical bifurcating surfaces · Cycloaddition reaction

Published as part of the special issue celebrating theoretical and computational chemistry in Spain.

J. M. Ramírez-Anguita · R. Gelabert (✉) · À. González-Lafont (✉) · M. Moreno · J. M. Lluch
Departament de Química, Universitat Autònoma de Barcelona, 08193 Bellaterra, Barcelona, Spain
e-mail: ricard.gelabert@uab.cat

À. González-Lafont
e-mail: angels@klingon.uab.es

1 Introduction

Transition State Theory (TST) represents a theoretical attempt at producing a consistent theory to compute, from first principles, the phenomenological rate constant of a chemical process. Compared to more costly and laborious approaches, like those based on classical trajectory integration or fully quantum approaches to rate processes, TST is a theoretical model whose level of detail is comparable to that of the observations it is trying to explain [1]. TST, in either its microcanonical or canonical versions, leads to convenient, easy to interpret closed-form equations that allow computing the rate constant as a function of a reduced set of molecular parameters. As is well known, it equates the local equilibrium one-way flux across a special surface in phase-space that separates reactant and products of reaction with the global net equilibrium flux reaching the products: the transition state (whence its name). Because of its simplicity and elegance, it has enjoyed a remarkable success in explaining in a quantitative way the rate of many chemical processes and, in one or another equivalent formulation, it belongs in the good books of the vast majority of experimental and theoretical chemists.

As any approximate theory, the validity of TST rests on that of the principles or assumptions from which it is derived, which in the case of canonical TST amount to four: (1) electronic and nuclear degrees of freedom are separable, (2) reactants are in thermal equilibrium according to a Maxwell–Boltzmann distribution, (3) motion along the reaction coordinate is separable at the transition state and can be treated classically, and finally, (4) any reactant or product system crossing the surface separating reactants and products—the transition state—does so only once. The large number of systems so far described using TST with success is an eloquent proof that

these assumptions hold for most cases [2]. However, it is unavoidable to encounter cases where TST runs into trouble when one of the premises is not holding. Violations of premise (1) are those in which the Born–Oppenheimer approximation is not applicable, a not uncommon situation in photochemistry but fairly rare in thermally activated processes. Violations of premise (2) include those processes with so-called non-statistical regimes, that is, processes occurring in time scales where the characteristic time is short enough to impede the onset of thermal equilibrium on the reactants. These can be found for instance in the form of radiation-triggered processes, including but not limited to intramolecular vibrational relaxation (IVR). Clause (3) fails in those not so uncommon systems where passage through the transition state surface occurs non-classically, mainly referring to classical tunneling in light-atom transfer reactions. However, for these cases, several approaches are available that semiquantitatively or quantitatively introduce a multiplicative factor, computed semiclassically, to correct the "classical" rate constant to account for quantum tunneling [2, 3]. Last but not least, clause (4), also known as the fundamental approximation, is seldom honored in full, and recrossing is a more or less omnipresent complication. To correct for this shortcoming improved versions of TST, namely the variational transition state theory (VTST) was developed by Truhlar and Garrett [4]. In VTST, the transition state surface is variationally optimized to minimize recrossing. Current implementations of VTST proceed by determining the minimum energy path (MEP), starting at the first-order saddle point in configurational space, to determine the normal surface to the MEP across which reactant one-way flux is minimal, even though other approaches exist.

Over the years, a trickle of cases have made their way into the scientific literature in which diverse authors have claimed that TST fails to correctly account for the experimentally observed reactivity—mostly the selectivity [5–8]. Often, these cases are connected with a specific topographical feature of the PES, namely a sequence of two saddle points connected by a MEP and without an intervening minimum. The MEP connecting both saddle points bifurcates at some intermediate point, leading to the diverse products of the reaction and being the second saddle point the lowest potential energy point in a MEP connecting these products. Should the first saddle point be close to the dynamical bottleneck, it is conceivable that none of the alternative (bifurcated) pathways will have neither an enthalpic nor an entropic barrier. If this were the case, predicting the branching ratio of such processes would be beyond the domain of VTST.

A particular case of the above would arise when the PES were symmetric, by which it is meant that the two products formed would be identical and the second saddle point would represent the interconversion of both—this kind of situation is common in symmetry breaking processes. Then, the dynamical bottleneck appears before symmetry is broken, but afterward motion along the orthogonal to the MEP becomes unbound and bifurcation appears *as the valley turns into a ridge*, which sets the name for the topographical feature: valley ridge inflection (VRI). A subtle case was studied through dynamical trajectory simulations: the H/D kinetic isotope effects (KIE) affecting the product rations in the ene addition of singlet oxygen ($^1\Delta_g^1O_2$) to tetramethylethylene [6, 7]. However, some of us proved [9] that after appropriately selecting the reaction paths, the generalized free energy profiles showed three energy peaks (the highest close to the highest energy saddle point and thus common to all products, and two others, one on each fork of the reaction path and of lesser entity). As such the process could be described as a dynamical system with many bottlenecks and had to be dealt properly with the generalization of the competitive canonical unified statistical (CCUS) model [10], thus proving that the existence of a VRI did not necessarily involve non-statistical dynamics behavior and that statistical theories for reaction rates can still be valid if a valid MEP can be found eventually connecting all products to the reactants [9].

The question remains open still as to what would happen with the non-symmetrical bifurcating surfaces. Ussing et al. [11] stated that in such cases, the MEP will not bifurcate, but there may be still trajectories leading to two distinguishable products. Thus, there being only one MEP, in the restricted sense of a path of minimum energy in all normal directions to it, it is concluded that no form of TST can predict the ratio of competitive product formation and that selectivity on such reactions must be studied via trajectory simulations in order to attain quantitative predictions. Indeed, in relation to this discussion, Ussing et al. studied the cycloadditions of ketenes with cyclopentadiene, see Fig. 1. Experimentally it is known that cycloaddition of

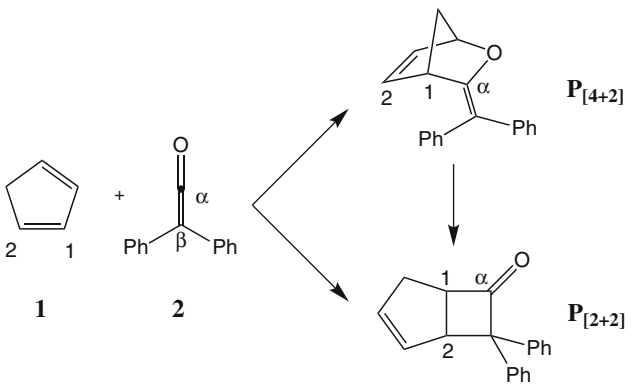

Fig. 1 Reaction under study: cycloaddition of cyclopentadiene **1** with ketene **2** to afford the [4+2] Diels–Alder product $\mathbf{P}_{[4+2]}$ and the product of a formal [2+2] addition, $\mathbf{P}_{[2+2]}$

ketenes with 1,3-dienes afford the product of a formal [2+2] cycloaddition instead of the [4+2] product after the Woodward–Hoffmann rules [12]. Yamabe et al. reported that the [4+2] product was formed initially to later rearrange into the cyclobutanone through a [3,3]-sigmatropic rearrangement of the [4+2] product [13, 14]. Ussing et al. carried out a combined experimental and theoretical study of the reaction depicted in Fig. 1. Through kinetic measurements, they established that $\mathbf{P}_{[2+2]}$ formed not only as a result of a [3, 3]-sigmatropic rearrangement *but also* directly. Indeed, they determined the values of the rate constants at −20 °C, these being 4.1×10^{-4} M^{-1} s^{-1} for the formation of $\mathbf{P}_{[4+2]}$ from reactants, 0.9×10^{-4} M^{-1} s^{-1} for the formation of $\mathbf{P}_{[2+2]}$ from reactants, and 2.9×10^{-5} s^{-1} for the formation of $\mathbf{P}_{[2+2]}$ from $\mathbf{P}_{[4+2]}$. The evidence that $\mathbf{P}_{[2+2]}$ forms directly was brought to the theoretical arena: A single saddle point connecting the reactants to $\mathbf{P}_{[4+2]}$ was located. Another saddle point connecting the reactants and $\mathbf{P}_{[2+2]}$ was found to lie 12.0 $kcalmol^{-1}$ higher in energy and thus termed irrelevant to the reaction and not responsible for the observed formation of $\mathbf{P}_{[2+2]}$. Revealingly, a third saddle point was found connecting $\mathbf{P}_{[2+2]}$ and $\mathbf{P}_{[4+2]}$, corresponding to the [3, 3]-sigmatropic rearrangement. Ussing et al. using quasi-classical trajectories starting at the saddle point linking reactants and $\mathbf{P}_{[4+2]}$ found that 1 out of 8 afforded *directly* $\mathbf{P}_{[2+2]}$ (being the experimental ratio 1:4.5, see above). This, together with the fact that the MEP of the reaction starting at the reactants avoided $\mathbf{P}_{[2+2]}$ completely, was taken as proof that no formulation of TST could explain the direct formation of $\mathbf{P}_{[2+2]}$ and that dynamical effects were at play that could only be accounted for by means of classical trajectories' simulations.

In this paper, it will be shown that adequate choice of the reaction path in this case also renders a good, almost quantitative description of the branching ratios within the framework of VTST and CCUS, conveniently applied to the characteristics of the system.

2 Computational details

To make comparison meaningful with the results of Ussing et al. [11], the same electronic structure methods have been employed here.

The Pople basis set 6-31+G(d,p) has been used [15]. Optimized geometries, energies and first and second derivatives of the energy have been computed using hybrid density functional theory [16–19]. The hybrid functional MPW1K [20] (modified Perdew–Wang one-parameter model for kinetics) has been chosen. The MPW1K functional is based on the Perdew–Wang exchange functional with Adamo and Barone's modified enhancement factor and the Perdew–Wang correlation functional. It has been tested against kinetic databases and has shown a good compromise between cost and accuracy. We note in passing that in their published work [11], Ussing et al. warned that this method of calculation might be overestimating the enthalpic barrier. As a result, it is to be expected that the computed rate constant values will have a significant offset from the experimental values.

Stationary points have been characterized by means of the analysis of the number of imaginary frequencies (this being one for first-order saddle points and zero for minima).

Dynamical calculations have been carried out using VTST. In the canonical variational transition state theory (CVT), the rate constant $k^{\mathrm{CVT}}(T)$ is obtained through minimization of the generalized rate constant $k^{\mathrm{GT}}(T, s)$ at temperature T along the reaction path, s:

$$k^{\mathrm{CVT}}(T) = k^{\mathrm{GT}}(T, s_*) = \min\left\{k^{\mathrm{GT}}(T, s)\right\} \tag{1}$$

where s denotes the distance along the MEP in an isoinertial mass-scaled coordinate system [3, 21] with a scaling mass equal to 1 amu, and s_* is the value of s that minimizes the generalized rate constant (or equivalently, that maximizes the generalized activation free energy) along the MEP at temperature T. The CVT rate constant is given by [2, 3]

$$k^{\mathrm{CVT}}(T) = \sigma \frac{k_B T}{h} \frac{Q^{\mathrm{GT}}(T, s_*)}{Q^{\mathrm{R}}(T)} \exp\left[-\frac{V(s_*)}{k_B T}\right] \tag{2}$$

where σ is the symmetry number, k_B and h are Boltzmann's and Planck's constants, respectively, $V(s_*)$ is the classical potential energy at s_* taken as energy origin the classical energy of reactants (i.e. excluding the zero point energy (ZPE) which is included in the partition functions), $Q^{\mathrm{R}}(T)$ is the reactant partition function per unit volume (with the energy origin placed at the reactants) and $Q^{\mathrm{GT}}(T, s_*)$ is the generalized transition state partition function with energy origin at $V(s_*)$ and excluding the reaction coordinate. Note that rotational symmetry numbers have been removed for all partition functions as they are included in σ. The symmetry number is computed as in [22–25]

$$\sigma(s) = \frac{n\sigma^{\mathrm{R}}}{\sigma^{\mathrm{GT}}(s)} \tag{3}$$

where n is the number of kinetically equivalent transition states, σ^{R} is the rotational symmetry number for the reactants (or the product of these symmetry numbers if there are two molecular reactants, as is the present case) and $\sigma^{\mathrm{GT}}(s)$ corresponds to the usual rotational symmetry number of the generalized transition state at s. In our applications, σ^{GT} is independent of s (because in practice it is approximated by the symmetry number at the saddle

point), and thus $\sigma(s)$ turns into a constant σ. The symmetry number has no effect on the dynamics behavior, but it may influence the value of the calculated rate constant.

Those minimum energy paths have been calculated in an isoinertial mass-scaled Cartesian coordinate system from the saddle point geometries by following the Page–McIver algorithm [26] at the MPW1K/6-31+G(d,p) level of theory. A step size *ds* of 0.05 bohr has been used in all cases. The second derivative matrices along the MEPs have been computed at every point. The generalized normal mode analysis along the MEP has been carried out in mass-scaled Cartesian coordinates. The reoriented dividing surface (RODS) algorithm [27] has been used to improve the generalized frequencies along the MEP and is necessary to obtain reliable generalized eigenvectors and frequencies.

Quasi-thermodynamic magnitudes have been computed by using the statistical thermodynamic formulation of partition functions within the ideal gas, rigid rotor and harmonic oscillator models. The imaginary frequency has been left out in the quasi-thermodynamic calculations of the transition states. Harmonic frequencies have been corrected for anharmonicity with a scale factor of 0.9515 [28] at the MPW1K/6-31+G(d,p) level, which also accounts for the deviation of this combination of functional and basis set from complete configuration interaction (CI). The standard state of 1 molecule $\times$ cm^{-3} has been adopted to give Gibbs free energies and rate coefficients at several temperatures.

The CUS theory [29] is a canonical generalization of the microcanonical unified statistical (US) theory [30] based on the probability branching analysis of Hirschfelder–Wigner [31]. To obtain the global reaction rate constant at the low pressure regime, the competitive canonical unified statistical (CCUS) theory [10] has been applied. This model has been proved to be valid if direct collisions do not occur [32].

Optimizations, frequency calculations and single-point energy calculations have been done with the Gaussian 03 package [33]. Minimum energy paths have been computed with the GaussRate 9.4 package [34] following the Page–McIver algorithm [26]. All direct dynamics calculations have been done with the PolyRate 9.4.3 [35] and GaussRate [34] computer programs.

3 Results and discussion

Ussing et al. [11] attempted a theoretical description of the potential energy surface at various levels of theory. Based on several criteria involving comparison of the predicted transition structure with those of the parent Claisen reaction at higher levels of calculation, the chosen methodology was DFT, with the MPW1K functional [20] and 6-31+G(d,p) basis set [15]. Exactly the same functional and basis sets have been adopted in our studies to make our comparisons with Ussing's results meaningful.

All stationary points reported by Ussing et al. were sought, located and characterized for the diphenylketene+cyclopentadiene reaction, and some geometrical data are gathered in Table 1 to enable discussion. We have reproduced correctly the energetics of the diphenylketene+cyclopentadiene reported by Ussing et al. [11]. Briefly, in what follows we summarize the energetics in terms of potential energy of the process. The most stable product of the reaction is the formal [2+2] product, $\mathbf{P}_{[2+2]}$, lying at -25.8 kcal mol^{-1} below reactants. A saddle point **SP0**, that Ussing et al. described as the saddle point linking directly reactants and $\mathbf{P}_{[2+2]}$, can be found lying very high in potential energy, 25.1 kcal mol^{-1} above reactants and thus having no relevance in the process. A second saddle point **SP1** is found at 13.1 kcal mol^{-1} above reactants, though. Building the MEP from **SP1** reveals that this saddle point links reactants with the [4+2] cycloaddition product, $\mathbf{P}_{[4+2]}$. Finally, a third saddle point, **SP2**, has been determined at 10.8 kcal mol^{-1} above reactants, and the corresponding MEP reveals that this structure corresponds to the saddle point in the interconversion of the $\mathbf{P}_{[4+2]}$ and $\mathbf{P}_{[2+2]}$ products, that is, the saddle point for the [3,3]-sigmatropic Claisen rearrangement. From this data, the logical conclusion seems to be [11] that TST would take **SP1** (or a structure close by) as dynamical bottleneck setting the rate for the global overall process, but would be at a loss to justify the experimentally proven to happen direct reaction of reactants to afford $\mathbf{P}_{[2+2]}$.

As a side note, even though because of its energy, **SP0** can be disregarded as playing any role in this reaction, for the sake of completeness the MEP starting at **SP0** was computed. It was found to lead, surprisingly, to an alternate [4+2] cycloaddition product in which the roles of diene and dienophile were reversed, $\mathbf{P}'_{[4+2]}$, not reported before. Along this MEP, a section with an orthogonal unbound mode was detected, but the exploration of the products it would lead to was not carried out because the high potential energy of the region rules it out as a possible factor in this reaction. It is possible however that following the MEP that bifurcates at this point would lead to the $\mathbf{P}_{[2+2]}$. Assuming that this saddle point is in some way involved in the formation of the $\mathbf{P}_{[2+2]}$ product [11], the branching ratio $\mathbf{P}_{[4+2]}/\mathbf{P}_{[2+2]}$ can be estimated to be of the order of $\exp[\Delta V^{\ddagger}/k_B T] = 2.3 \times 10^{10}$ at -20 °C, in disagreement with experiment.

Nevertheless, a closer look at the MEPs constructed is revealing of the features of the underlying PES. The branch of the MEP leading from **SP1** (at 13.1 kcal mol^{-1}) toward $\mathbf{P}_{[4+2]}$ has been analyzed to determine the Gibbs free

Table 1 Selected geometrical parameters (distances in Å, angles in degrees) for the relevant structures, and potential energy (V, in kcal mol^{-1}), relative to reactants at infinite distance

	1–2	cet–O	cet–α	α–2	O–1′
SP0	1.402	1.195	1.386	3.115	4.164
$\mathbf{P}'_{[4+2]}$	1.530	1.214	1.473	2.901	3.818
SP1	1.388	1.200	1.361	3.054	2.751
IP	1.442	1.236	1.385	2.963	2.508
$\mathbf{P}_{[4+2]}$	1.518	1.359	1.341	3.438	1.453
SP2	1.454	1.236	1.399	2.766	2.586
$\mathbf{P}_{[2+2]}$	1.549	1.195	1.535	1.568	3.859

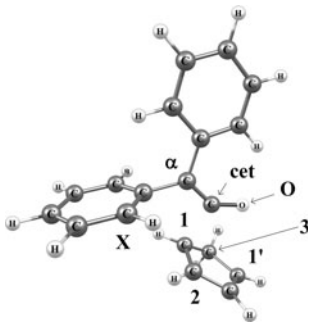

	cet–1	x–2	∠O-cet-1–3	∠O-cet-1–2	V
SP0	1.867	2.790	90.5	−157.4	25.1
$\mathbf{P}'_{[4+2]}$	1.522	1.527	55.1	171.1	−20.3
SP1	1.945	3.372	−14.5	92.8	13.1
IP	1.637	3.358	−12.9	93.2	11.1
$\mathbf{P}_{[4+2]}$	1.517	3.954	−35.4	67.2	−17.7
SP2	1.604	3.380	−6.7	98.7	10.8
$\mathbf{P}_{[2+2]}$	1.515	3.336	53.6	162.8	−25.8

The structures in the table are as follows: $\mathbf{P}_{[4+2]}$ is the 4+2 cycloaddition product (Woodward–Hoffmann allowed), $\mathbf{P}_{[2+2]}$ is the 2+2 cycloaddition product (Woodward–Hoffmann forbidden), $\mathbf{P}'_{[4+2]}$ is an alternative 4+2 cycloaddition product with the roles of diene and dienophile reversed, **SP0** is the saddle-point linking reactants and $\mathbf{P}'_{[4+2]}$, and presumably also $\mathbf{P}_{[2+2]}$; **SP1** is the saddle-point linking reactants and $\mathbf{P}_{[4+2]}$, **SP2** is the saddle-point that interconverts $\mathbf{P}_{[2+2]}$ and $\mathbf{P}_{[4+2]}$, and **IP** is an inflection point along the MEP linking **SP1** and $\mathbf{P}_{[4+2]}$ where one normal direction has become unbound

energy of activation. A necessary part of this process consists of obtaining the second derivative matrix of the potential at several points of the path, project the gradient component out and then obtain the harmonic frequencies, with which to compute the vibrational partition function and later on, the Gibbs free energy. At a point 4.3 bohr away from **SP1**, it was detected that one of the modes normal to the MEP attained a zero frequency, which turned imaginary and stayed so until a distance of 5.9 bohr was reached, a point from which it resumed with real values again until the end of the path was reached. The point at which this imaginary frequency appears has a relative potential energy of 11.1 kcal mol^{-1}. The fact that the second derivative of the energy at this point with respect to one of the normal directions to the MEP changes the sign of the curvature from positive to negative is a tell-tale factor relating this structure to those VRI in symmetrical surfaces. The situation here is different, because the surface is not symmetric and thus the slopes on either side of the inflection point need not be the same. The situation can be understood graphically from what is represented in Fig. 2. Because of this difference, we have decided to avoid this nomenclature and term it simply an inflection point, or **IP**. Some structural data of point **IP** are presented in Table 1. It is worth noting that the existence of this point has not been reported before for this reaction. The importance of its existence will be made clear soon.

A scrutiny of the data in Table 1 reveals that **IP** is very similar to **SP2**. This would mean that the stretch of the MEP that leads from **SP1** toward $\mathbf{P}_{[4+2]}$, and in particular the area where one of the normal directions has an associated imaginary frequency, is actually very close in energy and geometrically to the saddle point linking $\mathbf{P}_{[4+2]}$ and $\mathbf{P}_{[2+2]}$. Indeed, besides the sample of data presented in Table 1, Fig. 3 shows a graphical comparison of **SP2** and **IP**. It is clear that both are very similar; besides, distance O–1′ is slightly shorter in **IP** than in **SP2**, while for distances cet–1 and α–2 holds the opposite. A linear interpolation between both structures in mass-scaled coordinates yields a result of only 7.29 bohr, which taking into account the large number of heavy atoms is a clear indication of the large similarities, in a quantitative way, between **IP** and **SP2**.

Even though it is difficult to visualize the full landscape because of the sheer dimensionality of the problem, there are some data items that can help interpreting what is going on in this specific area of the PES. Along the MEP leading down from **SP1** to $\mathbf{P}_{[4+2]}$ motion along one of the normal

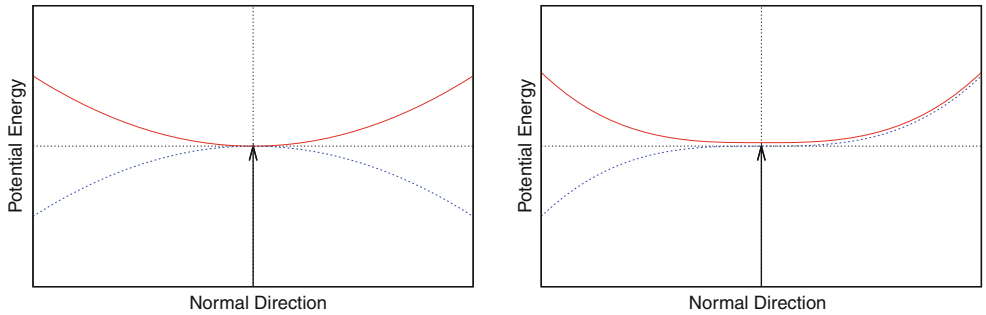

Fig. 2 A qualitative cut along the normal direction to the MEP undergoing the change of curvature, in a symmetric (*left*) and unsymmetric (*right*) surfaces. In both cases, the arrow pinpoints the location of the point of inflection. On a symmetrical surface before the change of curvature the profile along the normal direction to the MEP is concave (*red*) and after is convex (*blue*), and the slopes on both sides after the inflection point are the same. This is what has been known as a Valley Ridge Inflection (*VRI*). On an unsymmetrical surface, before (*red*) and after (*blue*) the inflection point, the picture is different because in the normal direction, the slopes on both sides are different. This must be the case of **IP**

directions to the MEP becomes increasingly loose until at some point, once **IP** is reached, it becomes unbound. However, being the PES asymmetric, the profile must resemble that of the right panel on Fig. 2: unbound to one side but very flat in energy to the other. The guess now and here is that the unbound end of this profile must lead toward **SP2**, the saddle point of the interconversion between $\mathbf{P}_{[4+2]}$ and $\mathbf{P}_{[2+2]}$. However, as noted above, the interval of the MEP for which the imaginary normal frequency is present is brief, $5.9 - 4.3 = 1.6$ bohr. Taking into account the large number of atoms that move and their masses, this interval corresponds to a very narrow bracket of geometry changes. After 5.9 bohr have passed along this path, the frequency becomes again real, meaning bound motion along the normal direction, a condition that will hold until $\mathbf{P}_{[4+2]}$ is reached. At this point, the potential energy has already sunk to 11.1 kcal mol^{-1} and immediately afterward plunges, which is a manifestation of the fact that the MEP has entered finally the $\mathbf{P}_{[4+2]}$ product valley, and hence, motion along the normal directions to the MEP must be bound. Figure 4 displays in a qualitative way these features.

The fact that the MEP is unbound for a certain window, for which it is very close both geometrically and energetically to **SP2**, suggests a possibility to apply rigorously VTST to try and explain the observed facts. In fact, the approach is very similar to that taken by some of us [9] to study branching ratios on a surface with a VRI. If a facile path (meaning short and energetically favorable) would link the **SP1**–$\mathbf{P}_{[4+2]}$ MEP to the area of **SP2**, then a competitive kinetic scheme would exist with a first common dynamical bottleneck (close to **SP1**), followed by a branched (competitive) scheme made up of (1) the rest of **IP**–$\mathbf{P}_{[4+2]}$ MEP, leading to the $\mathbf{P}_{[4+2]}$ product, and (2) a path (formally not a MEP) linking **IP**–**SP2** and followed by the MEP **SP2**–$\mathbf{P}_{[2+2]}$ and ending up at $\mathbf{P}_{[2+2]}$. If in such a scheme Gibbs free energy (G) maxima were to be found around **SP1** (serving the common stretch of path) and later on each of the branched paths (1) and (2) above, then an equivalent approach to that taken in [9] employing the competitive canonical unified statistical theory would be in order. These maxima are expected to exist: upon leaving **SP1** motion normal to the MEP becomes eventually unbound, which indicates that at least one of the frequencies contributing to G will vanish, making the area around **SP1** a candidate for a maximum of G. Along the stretch (1) above leading from **IP** to $\mathbf{P}_{[4+2]}$, the imaginary frequency that pinpoints the location of **IP** will disappear and as the MEP enters the region of the $\mathbf{P}_{[4+2]}$ a G barrier is also to be expected. And finally, stretch (2) will consist of a path—strictly not a

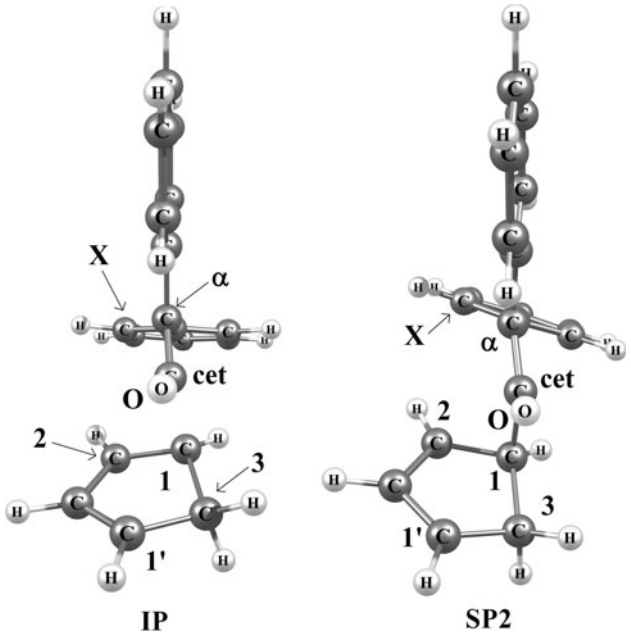

Fig. 3 A side-by-side picture of **SP2** and **IP**

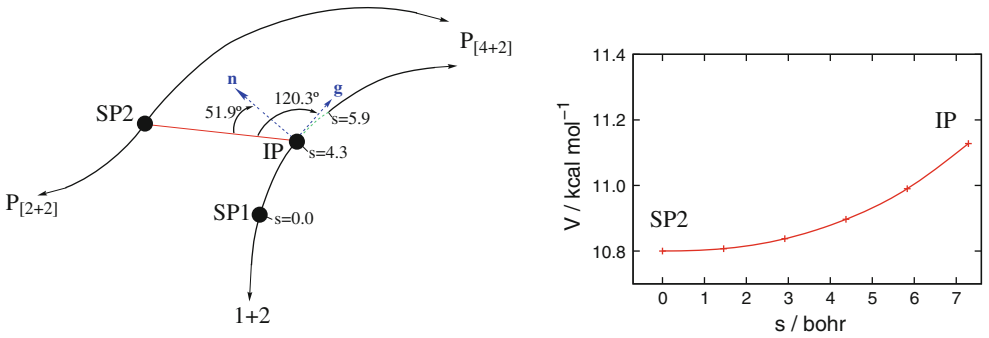

Fig. 4 Schematic representation of the surroundings of the inflection point **IP** (*left*). Solid black lines denote MEPs and can be identified through their reactants and products. Values of the reaction coordinate s in bohr. *Solid dots* identify relevant structures. Once the reactants follow the MEP and leave behind the saddle point **SP1** (marked with a reaction coordinate value of $s = 0$ bohr), the inflection point **IP** at $s = 4.3$ bohr is reached and a normal direction appears with an imaginary frequency. The MEP continues displaying such imaginary frequency normal mode until 5.9 bohrs have been traversed, where all frequencies become real and the MEP continues to $\mathbf{P}_{[4+2]}$: this stretch of the MEP with imaginary frequency normal mode is depicted in green. This path forms an angle of 120.3° with the MEP (indicated with g in the graph) and 51.9° with the normal direction with imaginary frequency (depicted with n). The linear path that links **IP** with **SP2** (*red*) is 7.29 bohr long and purely downhill path with a decrease of only 0.33 kcal mol^{-1} (*right*). Note that the coordinate origin in the potential energy profile on the *right* panel is placed at **SP2**

MEP—which has a gradient pointing either toward $\mathbf{P}_{[4+2]}$ or $\mathbf{P}_{[2+2]}$. In either case, the energy origin will lie very low making this stretch a low-G region compared to the stretch before **IP**, and because it leads after a short while to **SP2** and eventually to the $\mathbf{P}_{[2+2]}$ product valley, somewhere on its way again a G maximum is expected to appear.

The linear path that connects **IP** and **SP2** has been computed using mass-scaled coordinates. A purely downhill path has been obtained linking both structures. The gradient has been verified to be almost normal to the displacement vector and pointing always toward $\mathbf{P}_{[4+2]}$. Also, to help visualize the topography in the surroundings of this linear path, the angles it forms with the normal vector at **IP** associated to the unbound motion has been computed to be 51.9° and the angle determined by the linear path to the MEP linking **SP1** to $\mathbf{P}_{[4+2]}$ of 120.3°. Thus, the linear path linking **IP** and **SP2** starts off skewed from both the MEP and the normal unbound direction, and going somewhat backwards with respect the MEP. Figure 4 shows the potential energy profile along this linear path. It is easy to see that it is very flat, as only about 0.33 kcal mol^{-1} energy decrease is involved in going from the inflection point toward **SP2**.

A qualitative picture of the global reaction is depicted in Fig. 5. The global process is actually branched. A first common dynamical bottleneck appears close to **SP1**, **TS1**. After the inflection point **IP**, the path bifurcates leading either to $\mathbf{P}_{[4+2]}$ or $\mathbf{P}_{[2+2]}$. In both cases and for the reasons outlined above, a stretch of path with fairly low values of G appears ($\mathbf{M}_{[2+2]}$ and $\mathbf{M}_{[2+2]}$, respectively) followed by another dynamical bottleneck per branch, denoted by $\mathbf{TS}_{[4+2]}$ and $\mathbf{TS}_{[2+2]}$, respectively. Finally, the final products $\mathbf{P}_{[4+2]}$ or $\mathbf{P}_{[2+2]}$ are reached. Given that several bottlenecks

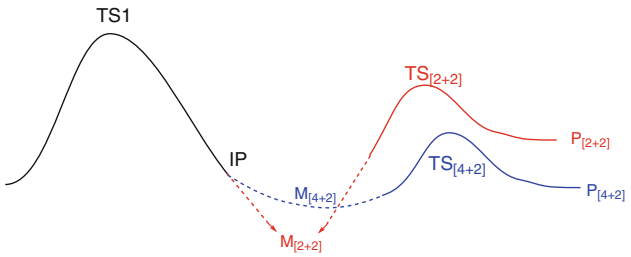

Fig. 5 Qualitative diagram depicting the generalized activation energy of the competitive process. Note that because it is an activation energy profile the identifier **TS1** (for transition state) is used even though it must be close to **SP1**. $\mathbf{M}_{[2+2]}$ and $\mathbf{M}_{[4+2]}$ denote the minima of Gibbs free energy found along each reaction path

are intervening, it is necessary to use the same generalization of the CCUS [10] we used before [9]. The branching ratio can be computed as

$$\frac{k_{[2+2]}}{k_{[4+2]}} = \frac{k_{\mathbf{TS}_{[2+2]}}}{k_{\mathbf{TS}_{[4+2]}}} \tag{4}$$

that is, the branching ratio can be computed from the ratio of the rate constants corresponding to the dynamical bottlenecks along each branch of the overall process. We have given the final result and refer the interested reader to the full derivation of Eq. 4 given in [9].

Gibbs free energies have been computed for the branched mechanisms using the PolyRate program [35] and are represented in Fig. 6. The values of $k_{\mathbf{TS}_{[2+2]}}$ and $k_{\mathbf{TS}_{[4+2]}}$ have been computed using the canonical variational transition state theory at the maximum values of G at several temperatures without any tunneling corrections, deemed to be unimportant for this reactions. The values $n = 4$, $\sigma_R = 4$ and $\sigma_{GT} = 1$ have been used (Eq. 3). Table 2

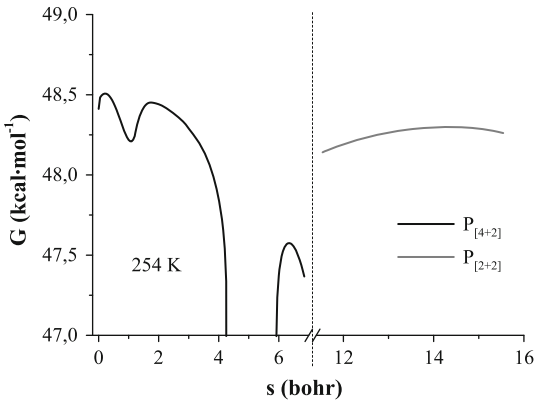

Fig. 6 Gibbs free energy profile at 254 K along the branched mechanism. Reaction coordinate origin is taken to be **SP1**. The part on the *left* is the common part of the mechanism and displays a dynamical bottleneck very close to $s = 0$ bohr. At 4.3 bohr **IP** appears and the branching occurs (corresponding to the curves on the right). At a path length of $s = 4.3$ bohr the structure **IP** appears, while at $s = 11.5$ bohr **SP2** is to be found. The hyatus between 4.3 and 5.9 bohr represents the stretch of the MEP running over a section with an imaginary frequency normal to the path on its way to $\mathbf{P}_{[4+2]}$ (*black*), and likewise that between 4.3 and 11.5 bohr identifies the stretch of the MEP running along the linear reaction path to $\mathbf{P}_{[2+2]}$ (*grey*). Both these stretches will have a very low G value as their origin lies at the bottom of the regions to which the modes with imaginary frequencies lead and thus are absent from the graph. Both branches display a local maximum of G unique to the specific product formed. Note that these G values are computed with a standard state of 1 molecule $\times$ cm^{-3}

shows the values of these rate constants and their ratio at several temperatures.

It is noteworthy that at all temperatures a dynamical bottleneck can be found for each of the branches in the mechanism (Table 2 has values for both constants at all temperatures). In all cases, the reaction producing $\mathbf{P}_{[4+2]}$ is always faster than that producing $\mathbf{P}_{[2+2]}$, which is what is observed experimentally. What is really surprising is the degree of agreement between the branching ratio computed and the value reported experimentally. At 254 K, the value computed is 3.95, which compares extremely well with that reported experimentally by Ussing et al. [11] of 4.1×10^{-4} M^{-1} s^{-1}/0.9×10^{-4} M^{-1} s^{-1} = 4.56.

Table 2 Canonical variational transition state theory rate constants corresponding to the dynamical bottlenecks along each branch of the global process (in molecule^{-1} cm^3 s^{-1}) and branching ratios as a function of temperature

T/K	$k_{\mathbf{TS}_{[4+2]}}$	$k_{\mathbf{TS}_{[2+2]}}$	$\mathbf{P}_{[4+2]}/\mathbf{P}_{[2+2]}$
238	1.65×10^{-28}	4.14×10^{-29}	3.98
254	9.27×10^{-28}	2.34×10^{-28}	3.95
272	5.09×10^{-27}	1.30×10^{-27}	3.92
297	3.88×10^{-26}	9.98×10^{-27}	3.88
298	4.17×10^{-26}	1.08×10^{-26}	3.88
324	2.46×10^{-25}	6.41×10^{-26}	3.84
349	1.06×10^{-24}	2.80×10^{-25}	3.80
374	3.80×10^{-24}	1.01×10^{-24}	3.76

4 Conclusions

Many cases in which TST has been claimed to fail have been proved to be tractable within the scopes of the theory. In general, the validity of TST is larger than usually believed.

The Woodward–Hoffmann rules for the cycloaddition reaction of ketenes with cyclopentadiene mandate that the [4+2] addition is allowed, whereas the [2+2] addition is forbidden. The potential energy values of the saddle points that connect reactants to either product provide a quantitative framework to these rules: they lead to a predicted ratio for $\mathbf{P}_{[4+2]}/\mathbf{P}_{[2+2]}$ on the order of $\exp[\Delta V^{\dagger}/k_B T] = 2.3 \times 10^{10}$ at -20 °C, assuming that **SP0** is connected somehow to the formation of $\mathbf{P}_{[2+2]}$ [11]. This prediction would come from considerations based solely on the initial structure of the reactants. The experimental measurements of Ussing et al. [11] at this temperature established a value of 4.56. Ussing et al. based on the evidence that the MEP connected only the reactants to the [4+2] cycloaddition product, found no way of applying TST to explain the experimental findings and undertook a classical trajectory simulation, with which it was possible to find that 1 out of 8 trajectories managed to find their way into the expected [2+2] product. Even though with poor statistics, this established the possibility to afford the [2+2] product when the MEP was not leading to it.

In this work, we have analyzed the process exploring the PES and applying the variational TST. We have found that the MEP that starts at the saddle point for the Woodward–Hoffmann allowed [4+2] cycloaddition reaches a plateau after losing about 2 kcal mol^{-1} potential energy. This plateau happens to be close to the entry channel to the valley for the Woodward–Hoffmann forbidden product [2+2]. Over this featureless expanse, it is possible to transfer from one to the other path as no energetic obstacles hinder it. This situation can be properly treated within the domain of the competitive canonical unified statistical theory (CCUS). The variational TST calculations render a value for the branching ratio at -20 °C of 3.95 amazingly close to the experimental value and in agreement also with the trajectory simulations of Ussing et al. [11] This provides an explanation within variational TST of this reaction's outcome and rules out the possibility that non-statistical effects be responsible for the observed reactivity.

In the specific reaction of cycloaddition of cyclopentadiene and ketene, this energy plateau represents in practice a means to dodge the rules of Woodward and Hoffmann, as

it is central in allowing transfer of reactive flux from the MEP of the Woodward–Hoffmann allowed [4+2] cycloaddition to the forbidden but thermodynamically more stable [2, 2] cycloaddition product.

In our opinion this work proves also that, although the structure of the reactants can make it possible to predict in most cases the outcome of a reaction, the topography of the potential energy surface is often very complex and unexpected kinetic behavior can be present. In those cases, an in-depth scrutiny of the different areas of the potential energy surface might be necessary to explain experimental behavior.

Acknowledgments The authors are grateful for financial support from the "Ministerio de Ciencia e Innovación" (project CTQ2008-02403/BQU) and from the "Generalitat de Catalunya" (project 2009SGR409). The use of supercomputer facilities at the "Centre de Supercomputació de Catalunya" (CESCA) is gratefully acknowledged.

References

1. Steinfeld JI, Francisco JS, Hase WL (1989) Chemical kinetics and dynamics. Prentice-Hall, Englewood Cliffs
2. Fernández-Ramos A, Miller JA, Klippenstein SJ, Truhlar DG (2006) Chem Rev 106:4518–4584
3. Truhlar DG, Isaacson AD, Garrett BC (1985) Theory of chemical reactions, vol 4. CRC Press, Boca Raton
4. Truhlar DG, Garrett BC (1980) Acc Chem Res 13:440–448
5. Bakken V, Danovich D, Shaik S, Schlegel HB (2001) J Am Chem Soc 123:130–134
6. Singleton DA, Hang C, Szymanski MJ, Meyer MP, Leach AG, Kuwata KT, Chen JS, Greer A, Foote CS, Houk KN (2003) J Am Chem Soc 125:1319–1328
7. Singleton DA, Hang C, Szymanski MJ, Greenwald EE (2003) J Am Chem Soc 125:1176–1177
8. Thomas JB, Waas JR, Harmata M, Singleton DA (2008) J Am Chem Soc 130:14544–14555
9. González-Lafont A, Moreno M, Lluch JM (2004) J Am Chem Soc 126:13089–13094
10. Hu WP, Truhlar DG (1996) J Am Chem Soc 118:860–869
11. Ussing BR, Hang C, Singleton DA (2006) J Am Chem Soc 128:7594–7607
12. Woodward RB, Hoffmann R (1969) Angew Chem Int Ed Engl 8:781–853
13. Yamabe S, Dai TS, Minato T, Machiguchi T, Hasegawa T (1996) J Am Chem Soc 118:6518–6519
14. Machiguchi T, Hasegawa T, Ishiwata A, Terashima S, Yamabe S, Minato T (1999) J Am Chem Soc 121:4771–4786
15. Frisch MJ, Pople JA, Binkley JS (1984) J Chem Phys 80:3265–3269
16. Kohn W, Becke AD, Parr RG (1996) J Phys Chem 100:12974–12980
17. Becke AD (1993) J Chem Phys 98:5648–5652
18. Gunnarsson O, Lundqvist BI (1976) Phys Rev B 13:4274–4298
19. Langreth DC, Perdew JP (1977) Phys Rev B 15:2884–2901
20. Lynch BJ, Truhlar DG (2001) J Phys Chem A 105:2936–2941
21. Fukui K (1981) Acc Chem Res 14:363–368
22. Pechukas P (1976) J Chem Phys 64:1516–1521
23. Villà J, Corchado JC, González-Lafont A, Lluch JM, Truhlar DG (1999) J Phys Chem A 103:5061–5074
24. Masgrau L, González-Lafont A, Lluch JM (2001) J Chem Phys 114:2154–2165
25. Fernández-Ramos A, Ellingson BA, Meana-Pañeda R, Marques JMC, Truhlar DG (2007) Theor Chem Acc 118:813–826
26. Page M, McIver JW (1988) J Chem Phys 88:922–935
27. Villà J, Truhlar DG (1997) Theor Chem Acc 97:317–323
28. See http://comp.chem.umn.edu/truhlar/index.htm#databases (accessed 4 Aug 2010)
29. Garrett BC, Truhlar DG (1982) J Chem Phys 76:1853–1858
30. Miller WH (1976) J Chem Phys 65:2216–2223
31. Hirschfelder JO, Wigner E (1939) J Chem Phys 7:616–628
32. Zheng J, Papajak E, Truhlar DG (2009) J Am Chem Soc 131:15754–15760
33. Frisch MJ, Trucks GW, Schlegel HB, Scuseria GE, Robb MA, Cheeseman JR, Montgomery JA Jr, Vreven T, Kudin KN, Burant JC, Millam JM, Iyengar SS, Tomasi J, Barone V, Mennucci B, Cossi M, Scalmani G, Rega N, Petersson GA, Nakatsuji H, Hada M, Ehara M, Toyota K, Fukuda R, Hasegawa J, Ishida M, Nakajima T, Honda Y, Kitao O, Nakai H, Klene M, Li X, Knox JE, Hratchian HP, Cross JB, Bakken V, Adamo C, Jaramillo J, Gomperts R, Stratmann RE, Yazyev O, Austin AJ, Cammi R, Pomelli C, Ochterski JW, Ayala PY, Morokuma K, Voth GA, Salvador P, Dannenberg JJ, Zakrzewski VG, Dapprich S, Daniels AD, Strain MC, Farkas O, Malick DK, Rabuck AD, Raghavachari K, Foresman JB, Ortiz JV, Cui Q, Baboul AG, Clifford S, Cioslowski J, Stefanov BB, Liu G, Liashenko A, Piskorz P, Komaromi I, Martin RL, Fox DJ, Keith T, Al-Laham MA, Peng CY, Nanayakkara A, Challacombe M, Gill PMW, Johnson B, Chen W, Wong MW, Gonzalez C, Pople JA (2004) Gaussian 03, Revision C.02. Gaussian, Inc., Wallingford
34. Corchado JC, Chuang YY, Coitiño EL, Truhlar DG (2006, June) GaussRate, version 9.4. See http://comp.chem.umn,edu/gaussrate (accessed 4 Aug 2010); University of Minnesota, Minneapolis
35. Corchado JC et al (2006 Nov) PolyRate, version 9.4.3. See http://comp.chem.umn.edu/polyrate (accessed 4 Aug 2010); University of Minnesota, Minneapolis